NILU: OR 68/2001

NILU: OR 68/2001
REFERENCE: O-99079
DATE: NOVEMBER 2001
ISBN: 82-425-1322-8

Final report for the project "Analysis of airborne- and surface measurements of the actinic flux":

Actinic fluxes during ALBATROSS

Arve Kylling

Final report for the project "Analysis of airborne- and surface measurements of the actinic flux": **Actinic fluxes during ALBATROSS**

Arve Kylling

November 27, 2001

1 Objectives

During the 1996 ALBATROSS field campaign measurements were made of the 2π downwelling actinic flux. In addition a number of other measurements were made, of particular interest here are the ozone column and the aerosol optical depth.

The objective of this report is to use these measurements together with a state of the art radiative transfer model to investigate the effect of clouds and aerosols on the actinic flux.

The instrumentation used to measure the actinic flux are described by (Hofzumahaus et al., 1999). Below the model simulations and subsequent data analysis are described.

Note that all measured data reported below has been multiplied by a factor of 1/1.35. This due to a sensitivity change of the spectroradiometer. For more information contact Dr. A. Hofzumahaus, Forschungszentrum Jülich, Germany.

All measured and simulated data presented and the software needed to perform the simulations and the subsequent analysis are available on the CD accompanying this report.

2 Simulation of the ALBATROSS measurements

The ALBATROSS actinic flux measurements were simulated using a state-of-the-art radiative transfer model and the best available set of input data.

2.1 Radiative transfer model

The UVSPEC radiative transfer model was used to simulate the measured spectra. UVSPEC is part of the libRadtran package available from http://www.libradtran.org. The UVSPEC model includes various methods for solving the radiative transfer equation. Here is used the discrete ordinate radiative transfer equation solver of (Stamnes et al., 1988) modified to account for the spherical shape of the atmosphere using the pseudo–spherical approximation (Dahlback and Stamnes, 1991). If not otherwise noted the pseudo–spherical radiative transfer equation solver was run in 8–stream mode.

To simulate a downwelling actinic flux spectrum, the actinic flux were calculated at high, 0.05 nm, spectral resolution. The resulting spectral actinic fluxes were convolved with the instrument slit function and interpolated to the center wavelength of the measurements. The solar zenith angle was assumed to be constant during the scan time which was typically less than a minute. Temperature dependent ozone cross sections were taken from (Bass and Paur, 1985) and the Rayleigh scattering cross section was calculated from the formula given by (Nicolet, 1984). The Earth-Sun distance during the cruise was accounted for. UVSPEC has been thoroughly compared

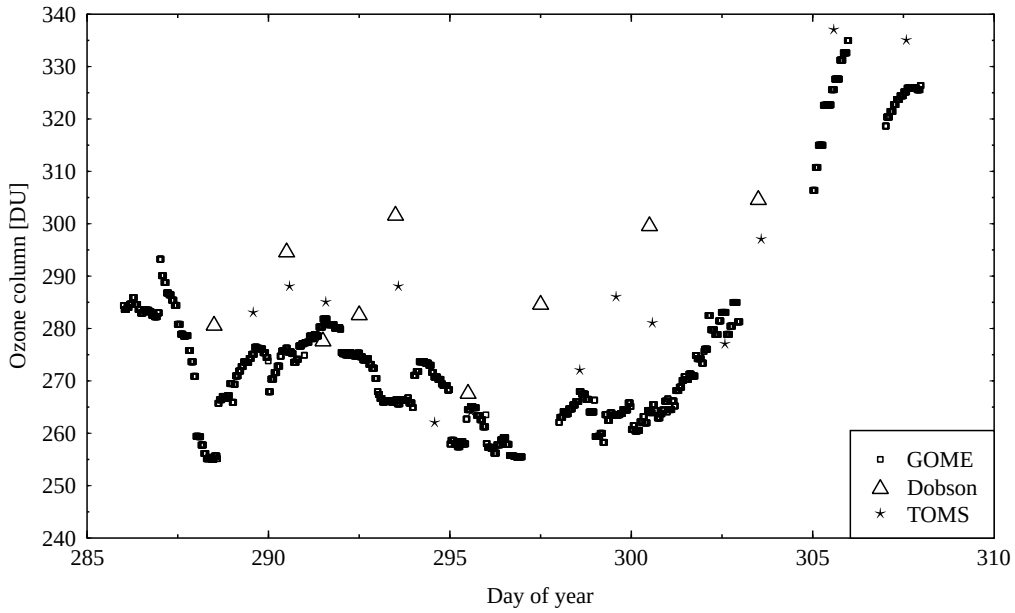

Figure 1: The ozone column from the GOME instrument, the TOMS instrument and onboard Dobson measurements (Herber 2001, private communication).

against landbased surface irradiance measurements (Mayer et al., 1997); (Kylling et al., 1998); (van Weele et al., 2000).

To solve the radiative transfer equation a number of input parameters are required, including the surface albedo, ozone column, aerosol optical properties and cloud information.

2.2 Surface albedo

The albedo of the ocean was set to 0.07, which is within the range (0.05-0.09) reported by (Doda and Green, 1980) for open ocean.

2.3 Ozone column and profile

The daily ozone values from the onboard Dobson instrument are shown as triangles in figure 1. Also shown in figure 1 is the ozone column as deduced from GOME measurements (squares) and TOMS (stars). The GOME and Dobson values differs considerably with the Dobson being higher by up to 25 DU. The TOMS and GOME data are closer, but differences up to 15 DU are present. For the present analysis the ozone values from the GOME instrument are used. For days when no ozone measurements are available Dobson values are used. For all simulations the US standard ozone profile was used (Anderson et al., 1986).

2.4 Aerosol optical properties

The aerosol optical depth was measured by a sun photometer. The optical depth at 350 nm as deduced from these measurements are shown in figure 2. The data are presented as daily averages. For some days data are missing due to persistent cloud cover.

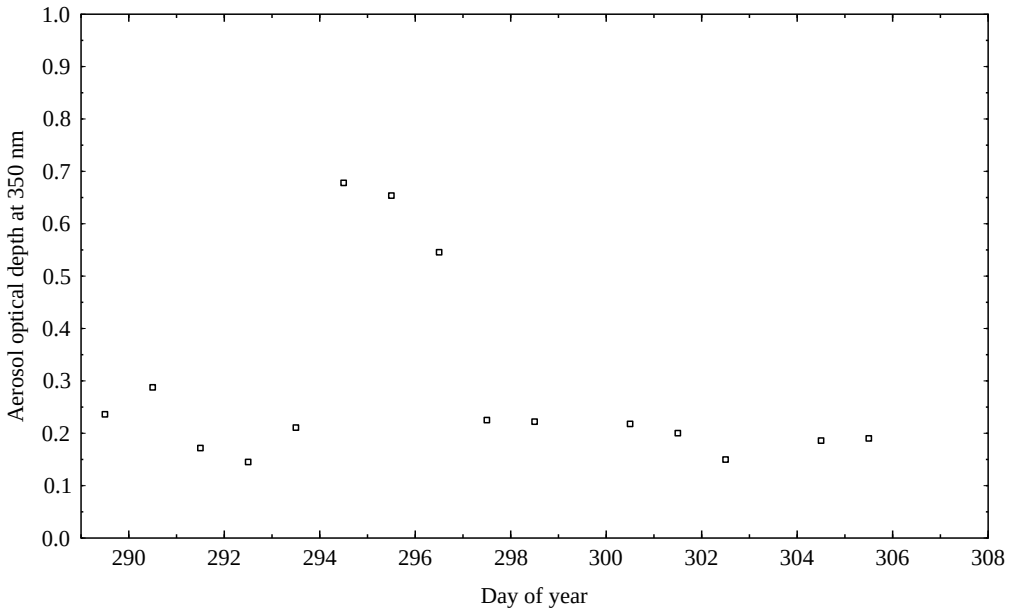

Figure 2: The aerosol optical depth at 350 nm as measured onboard Polarstern. Data courtesy of Dr. A. Herber, Alfred Wegener Institute, Potsdam, Germany.

The aerosol single scattering albedo was assumed to be 0.95 which is representative for areas with little pollution. The Heyney–Greenstein phase function was used with an asymmetry parameter of 0.7.

2.5 Cloud optical properties

From the actinic flux measurements an effective cloud optical depth was retreived as described in Appendix A. Using the retrieved cloud optical depth and an assumed effective droplet radius of 10 μm the cloud optical properties were calculated using the parameterization of (Hu and Stamnes, 1993). All clouds are assumed to be plane-parallel and reside between 2-4 km.

2.6 Sensitivity to ship movement

When measuring the 2π downwelling actinic flux the actinic flux head should be levelled. On a boat that is constantly in motion this is difficult to achieve. The instrument onboard Polarstern was fixed to the ship. As the ship rolled the instrument rolled with it. To test the sensitivity to ship rolling the radiance was calculated with a polar angle resolution and an azimuthal resolution of 1°. The solar zenith angle was 10° and in the south. The aerosol loading was low (day 301, see Figure 2). The actinic flux was calculated from the radiance distribution assuming perfect angular response of the input optics. Roll angles between 0 and 20° were considered. The ratio of the diffuse actinic flux for a given angle to the diffuse actinic flux when the ship is levelled is shown in Figure 3. Rolling movements of the ship decrease the diffuse actinic flux for all roll angles. Even for large roll angles of up to 20° the decrease in the diffuse actinic flux is relatively small ($< 7.\%$). For an isotropic radiation distribution the decrease would be 11% for a roll angle of 20°. The effect on the measured actinic flux must include the direct actinic flux as well. As long as the input optics sees the direct sun including the direct actinic flux will make the error

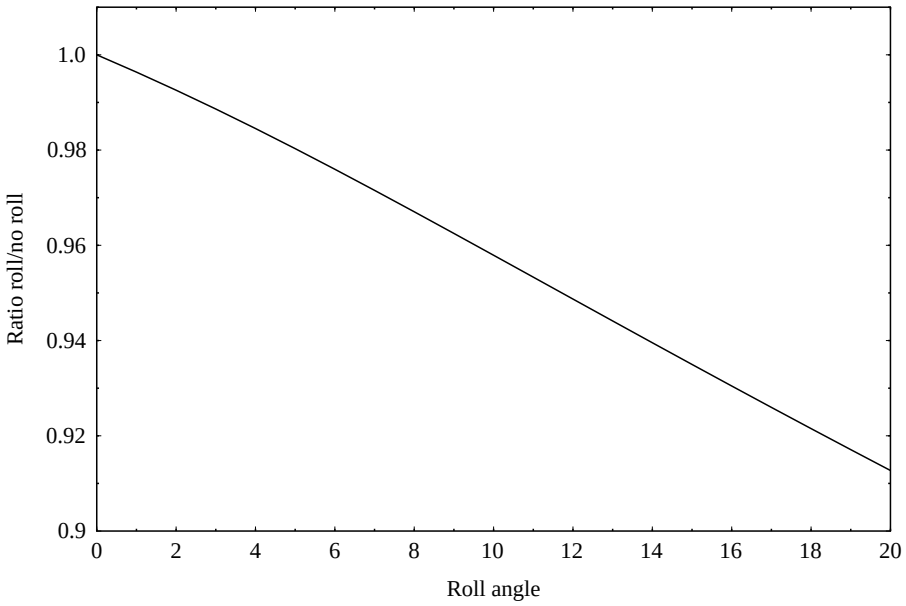

Figure 3: The ratio of the actinic flux for a given angle to the actinic flux when the ship is levelled. The direct actinic flux is not included.

on the total actinic flux even smaller. Hence, the uncertainty in the actinic flux measurements due to rolling of the ship are considered to be small compared with the other measurement and modelling uncertainties relevant for the analysis presented in this report. Effects of ship motion will thus be neglected.

3 Results

As a first check of the performance of the model it is compared with measurements made under cloudless conditions, but with aerosols present. Next the impact of aerosols are investigated by comparing simulations with and without aerosols. Finally cloud effects are quantified by comparing cloudfree simulations with simulations including clouds where the optical properties of the clouds are derived from measurements.

3.1 Cloudless sky results

Clear sky days and periods were identified by looking at the diurnal behaviour of the actinic flux. Day 301, 27 October, is the only day which is nearly cloudfree. In Figure 4 the actinic flux is shown at selected wavelengths as a function of the time of the day. The ripples in the afternoon indicate presence of some patchy clouds while the smoothness earlier in the day is typical for cloudless conditions. The same data are shown in Figure 5 as a function of the solar zenith angle.

Each measured spectrum was simulated using the uvspec model as described above. For the cloudless situation aerosols, but no clouds, were included in the simulations. The ratio between the measurement and the simulations for day 301 are shown for selected wavelengths in Figure 6 as a function of time and in Figure 7 as a function of solar zenith angle.

Examples of indvidual spectra at selected solar zenith angles are shown in Figure 8. In Figure 9

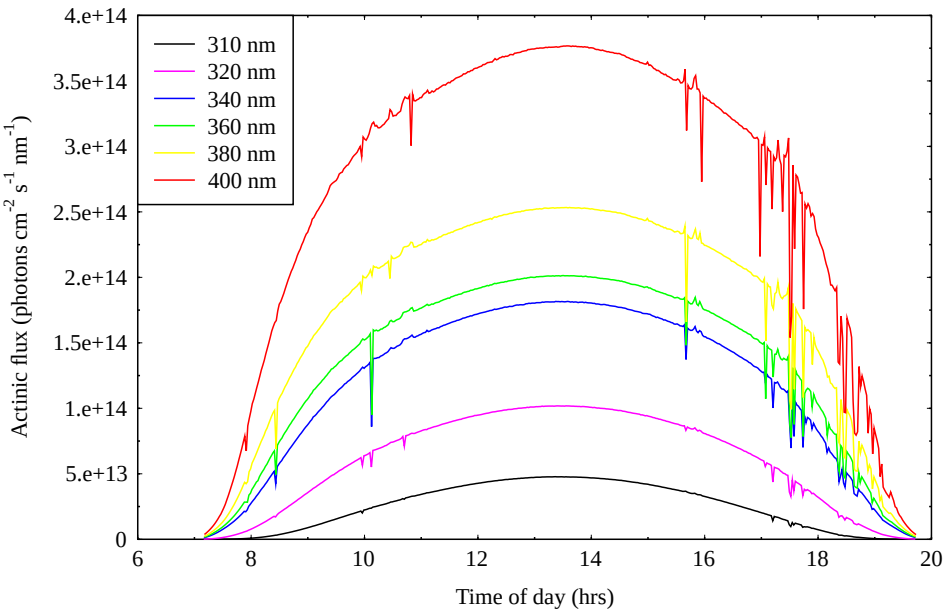

Figure 4: The measured actinic flux at various wavelengths for day 301 (27 October)

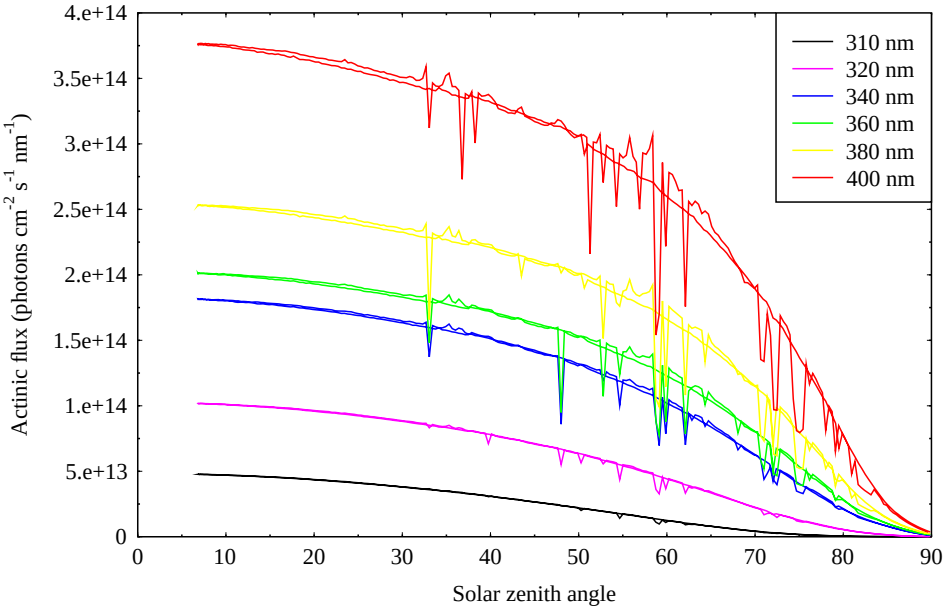

Figure 5: Similar to figure 4, but as a function of solar zenith angle.

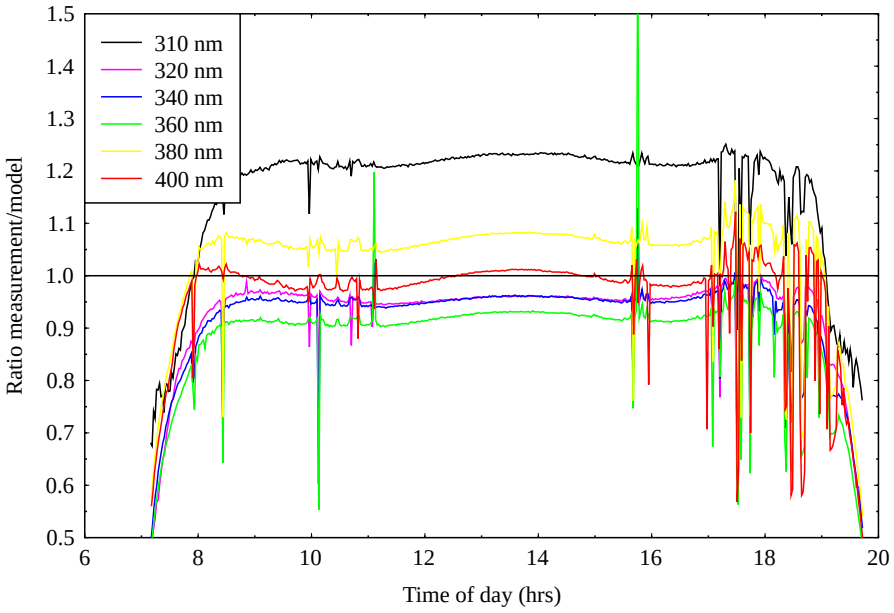

Figure 6: The ratio between measurement and model for day 301.

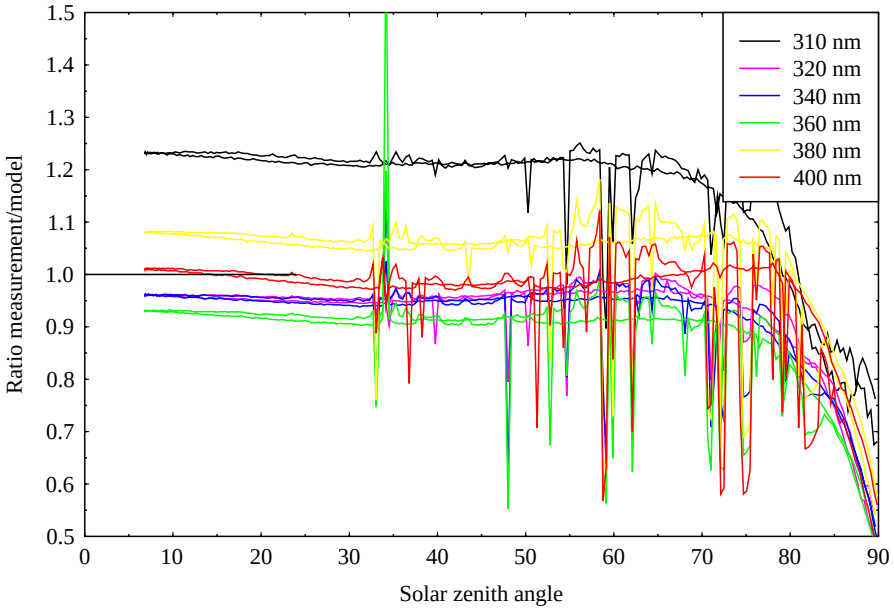

Figure 7: Similar to figure 6, but as a function of solar zenith angle.

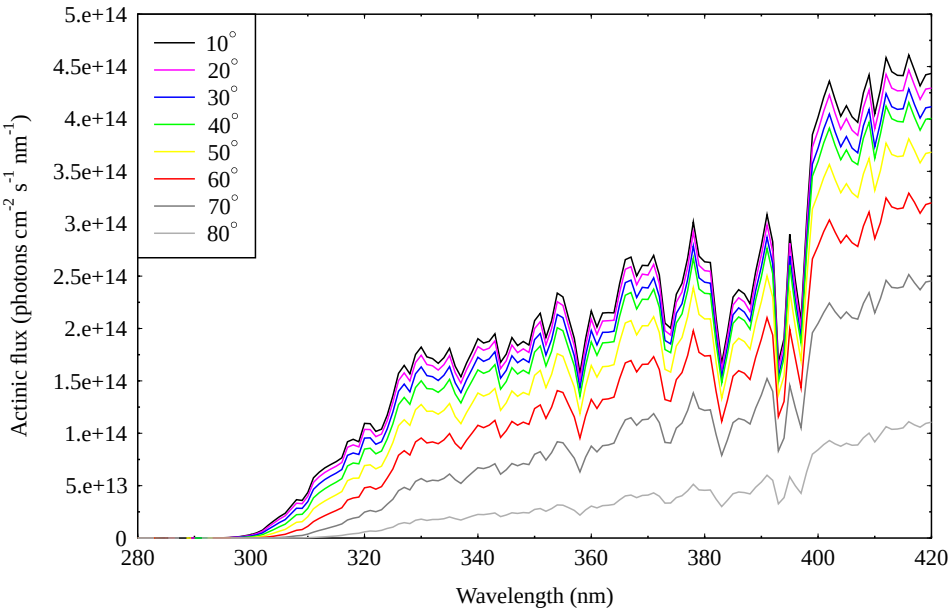

Figure 8: Measured spectra at selected solar zenith angles from the cloudless day 301.

is shown ratio of these spectra with simulated spectra.

Generally the agreement between the model and the measurements are within ±10%, Figures 6, 7 and 9. However, for large solar zenith angles and short wavelengths the measurement and model results exhibit larger differences. For wavelengths shorter than 310 nm the model is larger than the measurements for solar zenith angles larger than 75° (Figures 9 and 7). For smaller solar zenith angles the model and measurement agree for wavelengths above 340 nm. For shorter wavelengths the model gets increasingly larger than the measurements. This increasing discrepancy may be explained by a too small ozone column for the model simulation. The above comparison of the ozone column from TOMS, GOME and the onboard Dobson revealed large differences that may explain the model/measurement differences for shorter wavelengths.

For solar zenith angles larger than 75° the model gets increasingly larger than the measurements, Figure 7.

The measured and simulated spectra agree well with respect to their wavelength scales, see Figure 9 and also comments by (Hofzumahaus et al., 2001).

3.2 Aerosol effects

The aerosol loading was low during most of the ALBATROSS campaign. This is evident from both onboard sun photometer measurements and satellite data. The optical depth at 350 nm is shown in Figure 2. The optical depth is typically around 0.2. For comparison the Rayleigh optical depth at 350 nm is around 0.63. However, between days 294 (20 October) and 296 (22 October) Polarstern passed through an aerosol "cloud" of Saharan dust. This "cloud" is clearly seen in the aerosol index as estimated from the Earth Probe Toms instrument, Figure 10. On day 296 Polarstern was at 4.68°N and 26.53°W at noon. Hence in the middle of the aerosol "cloud" seen west of Africa. On the following day Polarstern travelled south and was at 0.61°N and 25.66°W at noon and thus south of the aerosol "cloud", Figure 11. While within this aerosol "cloud" the

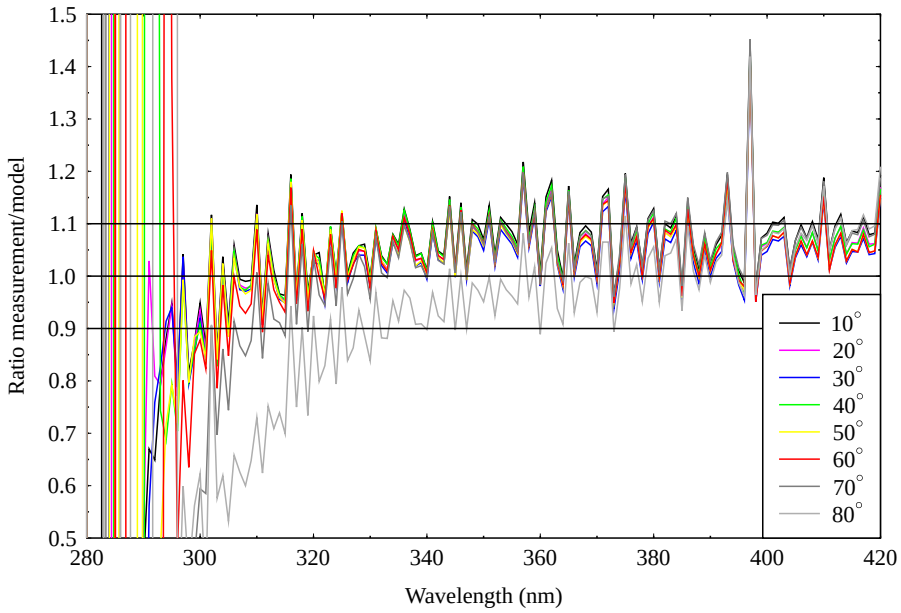

Figure 9: Ratio between the measured spectra shown in Figure 8 and simulated spectra.

aerosol optical depth reached values of up to 0.68.

To estimate the radiative effect of the aerosol cloudless simulations were performed with and without aerosols. In Figure 12 is shown the ratio,$E_{tot}^{aero}/E_{tot}^{clear}$ of model simulations with aerosols to simualations without aerosols, that is Rayleigh scattering only. The wavelength is 380 nm. The same data is shown in Figure 13 as a function of the solar zenith angle. The rather low aerosol optical depth outside the aerosol "cloud" reduces the actinic flux by 3-12% depending on solar zenith angle. Inside the aerosol "cloud" the actinic flux is reduced by up to 30%. These reductions are similar to those reported for irradiance measurements made in June 1996 in Greece (Kylling et al., 1998).

The effect of the aerosol is solar zenith angle dependent, with the reduction being largest between 70-80° and decreasing for smaller and larger solar zenith angles. For small solar zenith angles the direct radiation dominates. If τ_a (τ_c) is the total optical depth of the atmosphere with (without) aerosol at a given wavelength then $\tau_a > \tau_c$ and the aerosol reduce the actinic flux. As the solar zenith angle increase the direct contribution to the total actinic flux decrease. The direct contribution is always smaller for an aerosol loaded sky. Also the direct radiation decreases more rapidly with solar zenith angle for an aerosol loaded sky. Hence, the decrease in the ratio in Figure 13 for solar zenith angles up to 70-80°. For larger solar zenith angles the diffuse radiation, E_{dif} dominates. Since E_{dif}^{aero} is a larger portion of E_{tot}^{aero} than E_{dif}^{clear} is of E_{tot}^{clear} the ratio $E_{tot}^{aero}/E_{tot}^{clear}$ increases for large solar zenith angles.

3.3 Cloud effects

To get a first estimate of the radiative effect of clouds, quantitative information on the optical properties of clouds is needed. (Stamnes et al., 1991) described a method to deduce the effective cloud optical depth from irradiance measurements. By effective cloud optical depth is meant the optical depth that when used in the model best reproduces the measurements. Hence, the

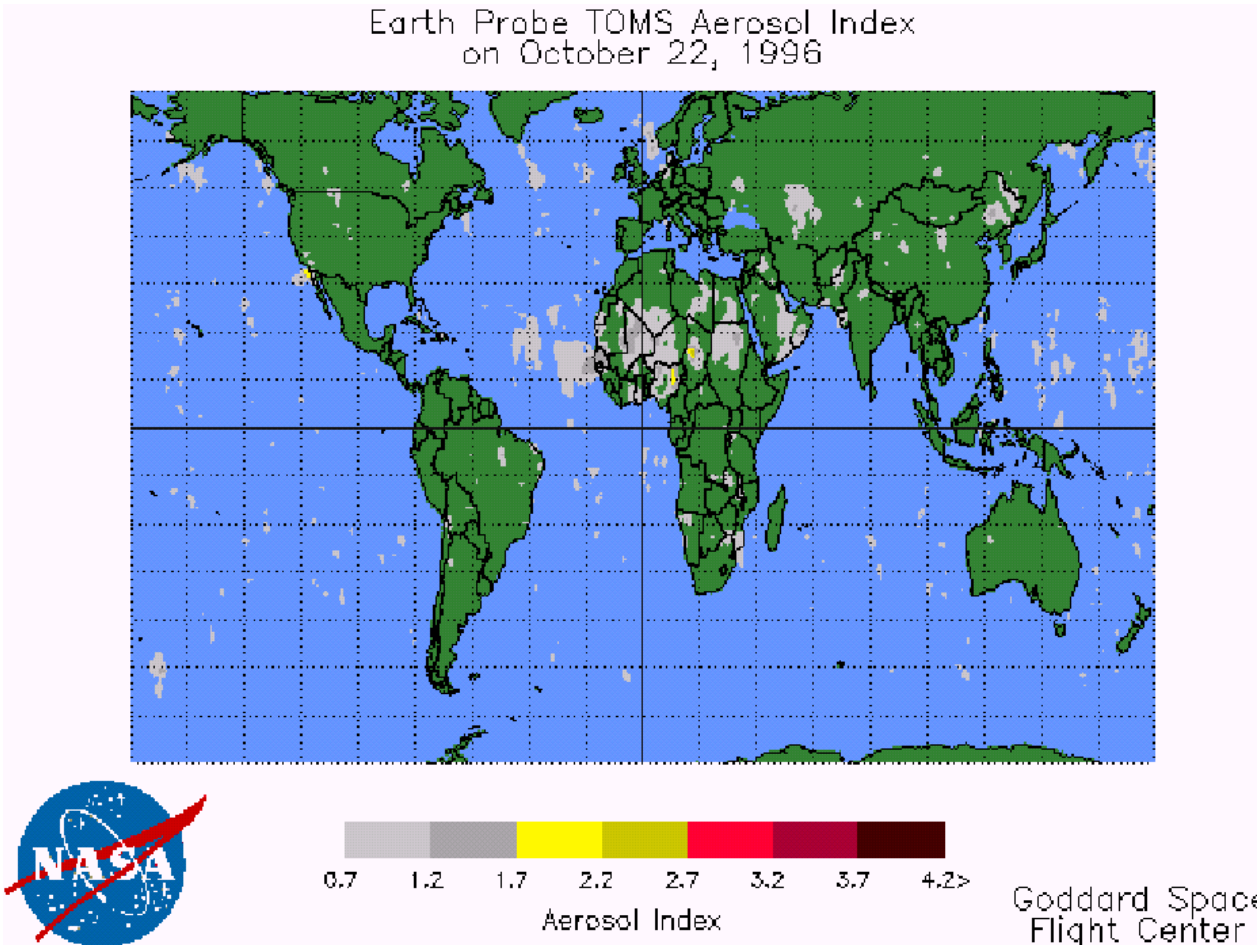

Figure 10: The Earth Probe Toms Aerosol Index for day 296, 22 October. The figure is taken from the TOMS home page (toms.gsfc.nasa.gov).

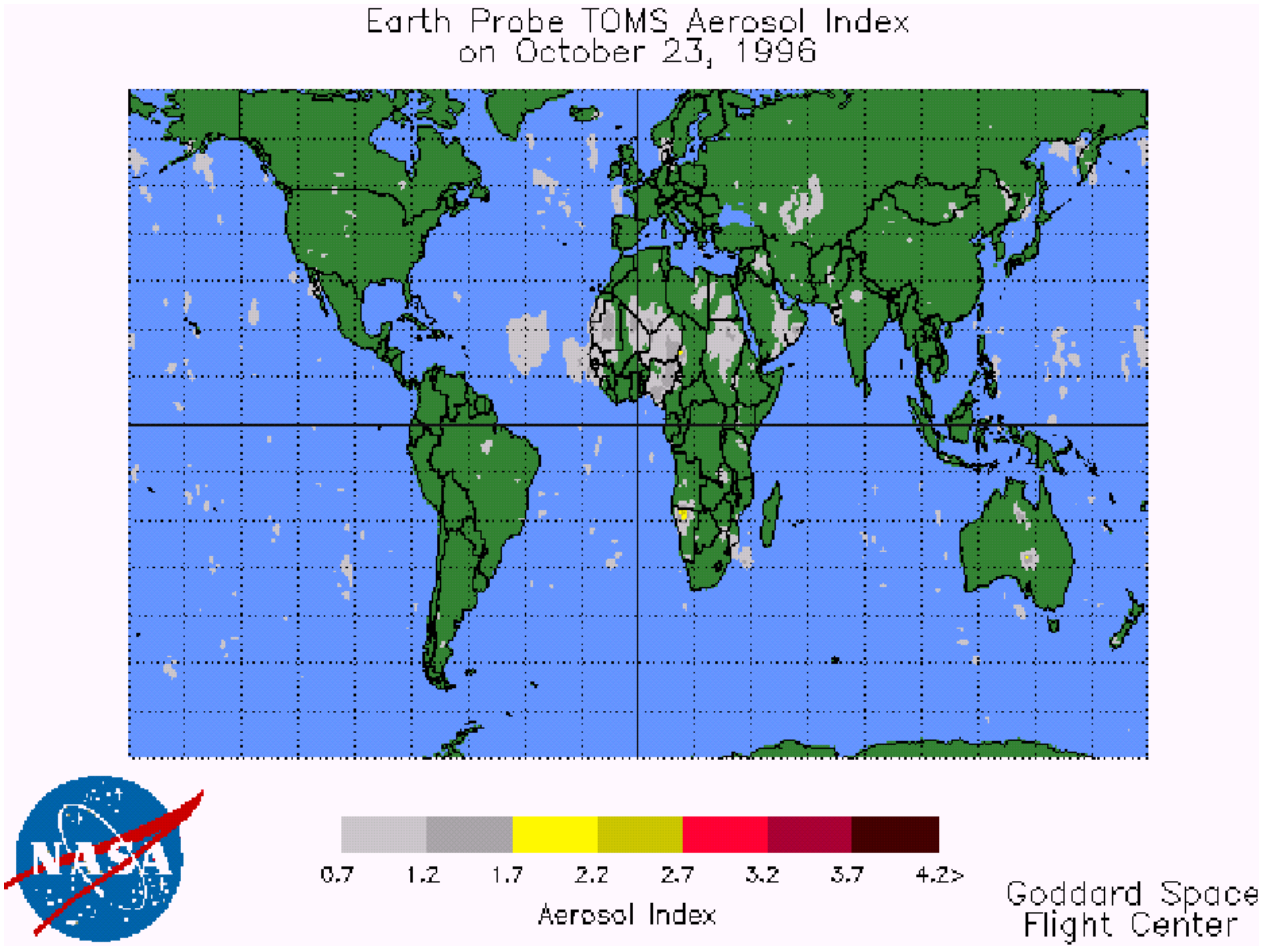

Figure 11: Similar to figure 10, but for day 297, 23 October.

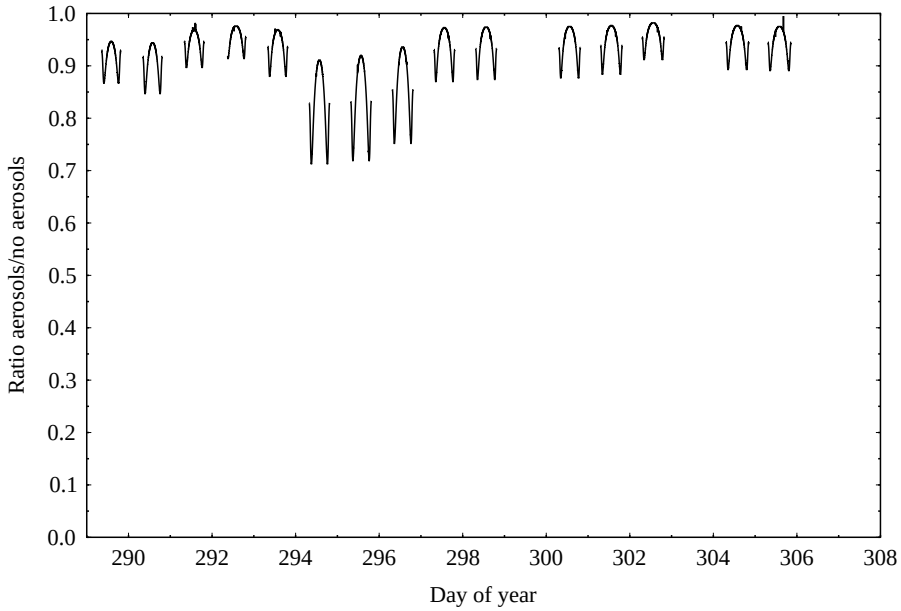

Figure 12: Ratio of model simulations with aerosol to simulations without aerosol as a function of time.

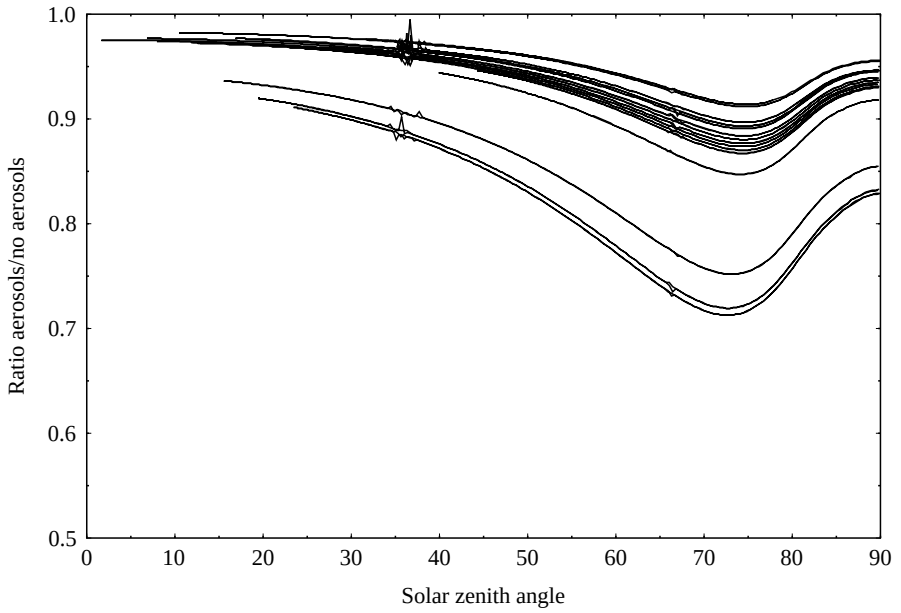

Figure 13: Same as Figure 12, but as a function of solar zenith angle. Note also change in y-axis scale.

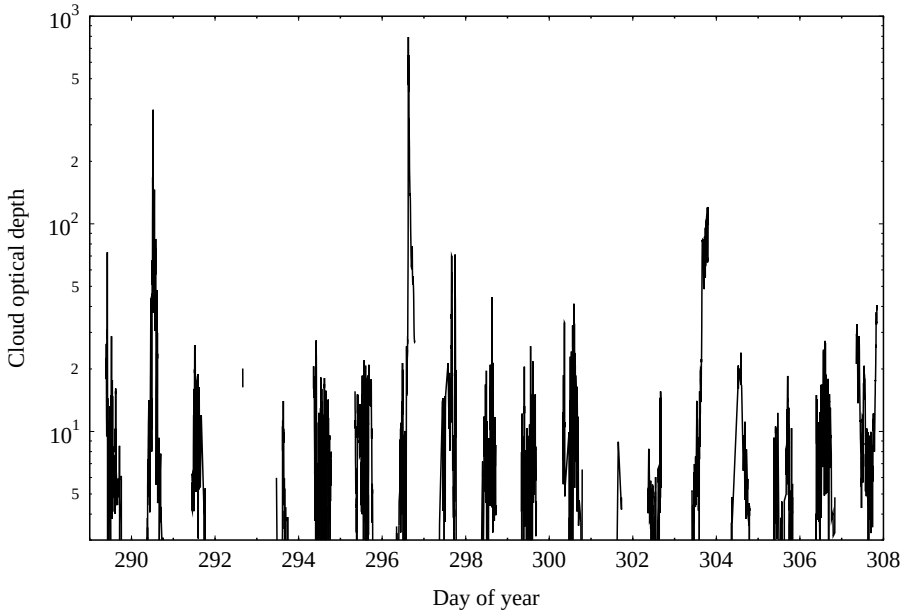

Figure 14: The effective cloud optical depth retrieved from the actinic flux measurements as a function of time. Clouds with optical depth smaller than 3 are not included due to uncertainties in the cloud retrieval.

effective cloud optical depth includes both aerosol and cloud optical depths. No suitable irradiance measurements are available from the ALBATROSS campaign. Instead an attempt was made to use the actinic flux to derive the effective cloud optical depth. However, for small cloud optical depths, $\tau < 3$, this method yields two answers for small solar zenith angles, see Appendix A. Hence, only effective cloud optical depths larger than 3 are included in the subsequent analysis.

The effective cloud optical depth was retrieved from actinic flux measurements centered at 380 nm and averaged with a triangular function with a FWHM of 5 nm. In Figure 14 the retrieved optical depth is shown as a function of time. The optical depth exhibit large variability with the largest value of $\tau = 600$ on day 296, 22 October, when Polarstern was about 4° north of the equator, or in the intertropical convergence zone (ITCZ).

The frequency distribution of the cloud optical depth is shown in Figure 15. There is an abundance of relatively thin clouds with optical depths smaller than 20 while thick clouds are relatively sparse. The present data is a snapshot of the conditions as the ship travels. Longterm measurements at selected latitude bands would most likely give different frequency distributions.

The cloud optical depths in Figure 14 were used as input to the model to check how good the cloud retrieval is. The ratio between these model simulations and the measurements are shown in Figure 16 for selected wavelengths. Note that no cloudless data are present in Figure 16. As the effective cloud optical depth was retrieved for 380 nm the comparison at this wavelength should be one. The differences observed at large solar zenith angles are caused by differences in the plane-parallel radiative transfer equation solver used to make the optical depth versus actinic flux tables, and the pseudo-spherical solver used for the simulations. The comparison at 340 nm constitutes an independent check of the approach and gives an overall idea of the uncertainty of retrieving the cloud optical depth this way.

To quantify the reduction in the actinic flux due to clouds the cloudy simulations were compared

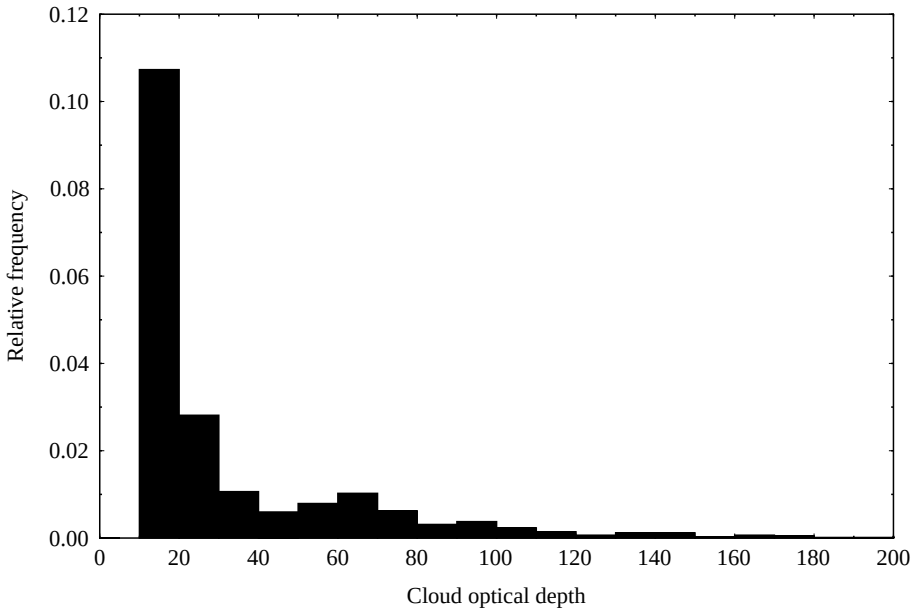

Figure 15: The relative frequency of clouds with a given optical depth. Clouds with optical depth smaller than 10 are not included due to uncertainties in the cloud retrieval.

to the cloudless simulations. In Figure 17 the reduction of the actinic flux at 380 nm due to clouds compared with a cloudless sky is shown as a function of time. The same data is shown as a function of olar zenith angle in Figure 18. The large spread for a single optical depth is due to solar zenith angle variations. In Figure 19 subsets of the same data are shown as a function of the solar zenith angle. Each subset consists of data with effective cloud optical depth within a specified interval. For a given effective cloud optical depth the reduction in the actinic flux compared to the cloudless sitation increases as the solar zenith angle increases. For large solar zenith angles the direct radiation will penetrate shorter into the cloud and hence has a greater likelihood to be scattered upwards out of the cloud. Thus the reduction of the ratio in Figure 19 with increasing solar zenith angle.

4 Photodissociation of ozone: J[O(^{1}D)]

Given an actinic flux spectrum a number of photodissociation rates may be readily calculated provided the appropriate cross section and quantum yields are available. One photodissociation rate of particular importance and interest in tropospheric chemistry is the J[O(^{1}D)] photodissociation rate of ozone. It was calculated from the actinic flux measurements, ozone cross section from (Bass and Paur, 1985) and ozone quantum yield of (Talukdar et al., 1998). The time evolution of the J[O(^{1}D)] photodissociation rate is shown in Figure 20. The dependence on solar zenith angle is shown in Figure 21.

The general picture of how the J[O(^{1}D)] photodissocation rate is affected by aerosols and clouds, is similar to that presented in Figures 12-13,17-19 for a wavelength of 380 nm. However, the J[O(^{1}D)] photodissocation rate has a shorter effective wavelength where the proportion of diffuse light is larger than at 380 nm. Hence, with more of the radiation already diffuse, the aerosol and cloud effect is somewhat smaller.

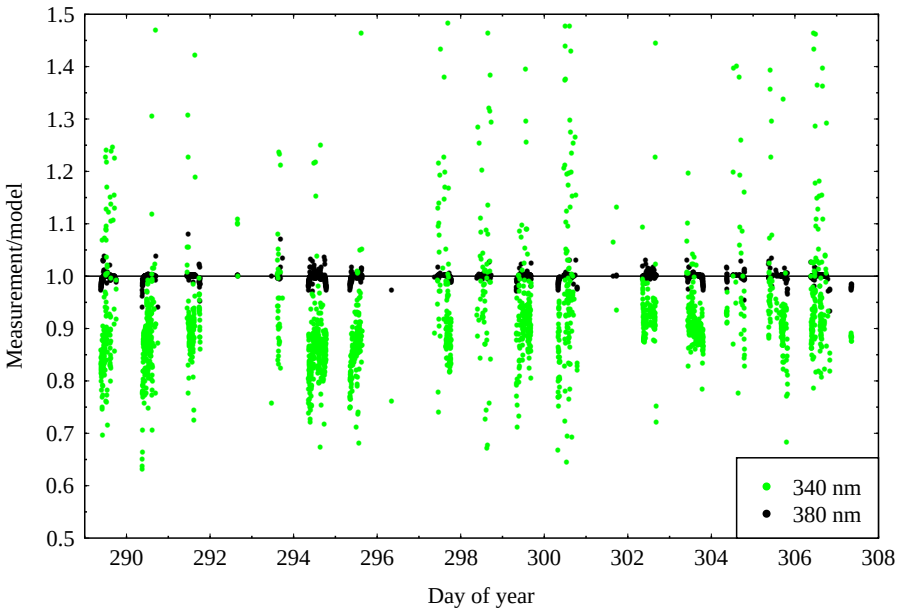

Figure 16: The ratio between the measured and modelled (with clouds) actinic flux for effective cloud optical depths larger than 3.

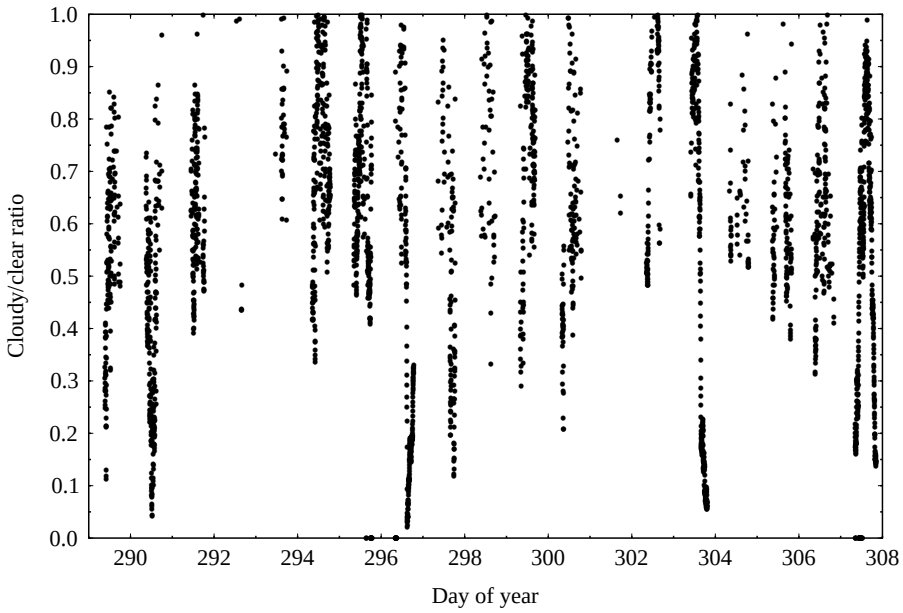

Figure 17: The reduction in the actinic flux at 380 nm due to clouds compared with a cloudless sky.

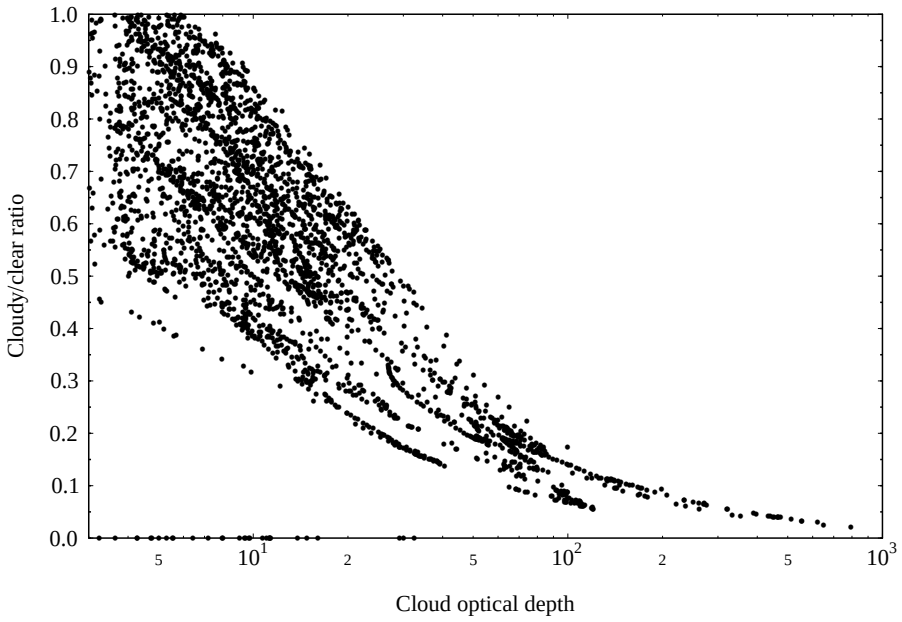

Figure 18: The reduction in the actinic flux at 380 nm due to clouds as a function of effective cloud optical depth.

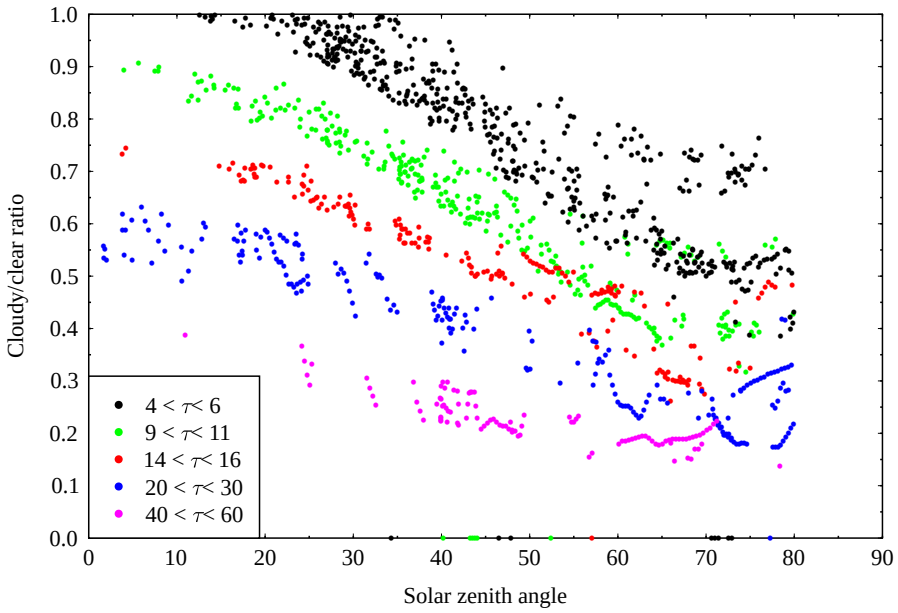

Figure 19: The reduction in the actinic flux at 380 nm due to clouds as a function of solar zenith angle for a few selected effective cloud optical depths τ.

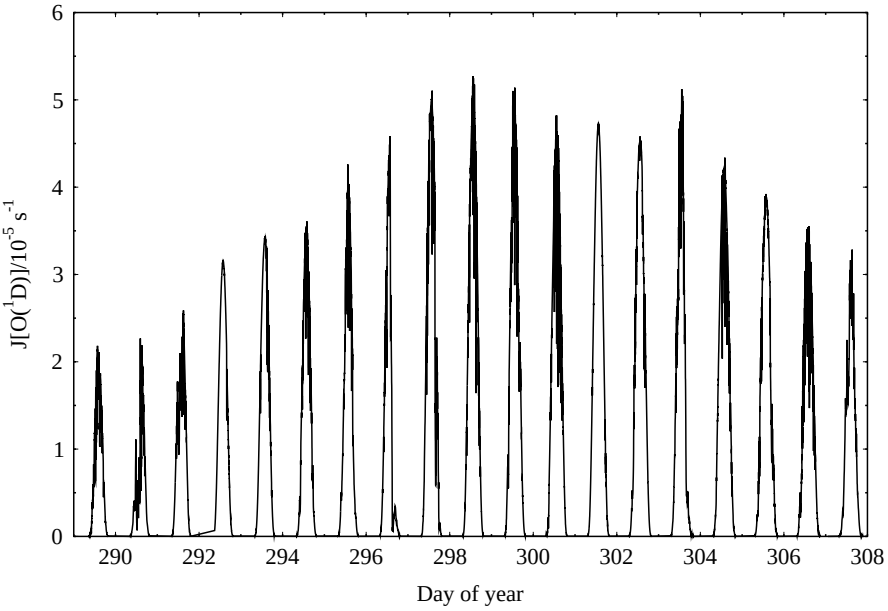

Figure 20: The J[O(^{1}D)] photodissocation rate as a function of time. The photodissociation rate was calculated from the actinic flux measurements, ozone cross section from (Bass and Paur, 1985) and ozone quantum yield of (Talukdar et al., 1998).

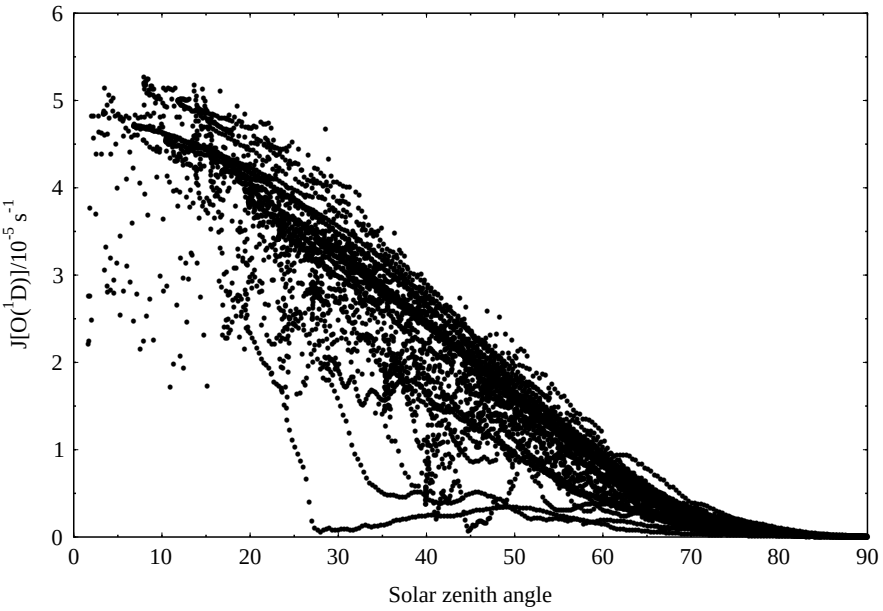

Figure 21: Similar to Figure 20, but as a function of the solar zenith angle.

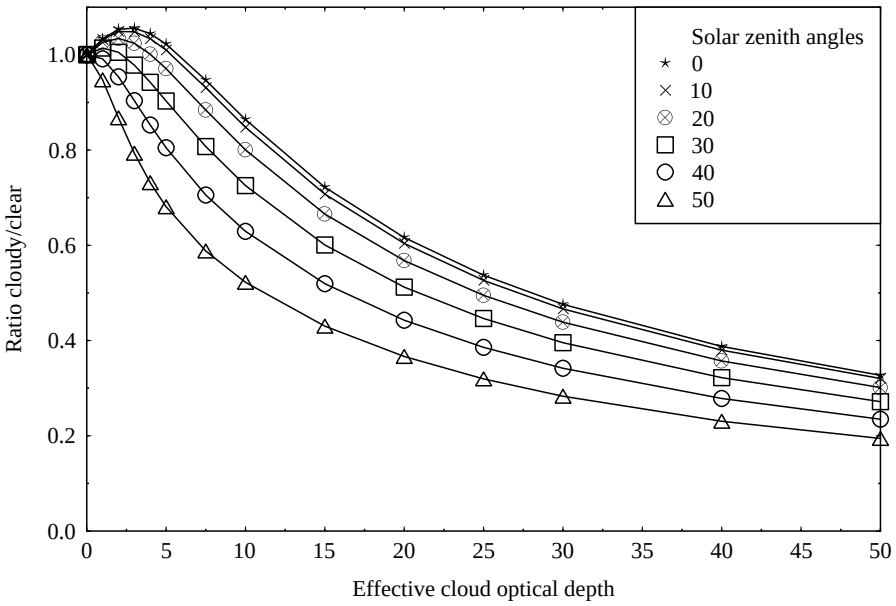

Figure 22: The actinic flux at 380 nm as a function of effective cloud optical depth for various solar zenith angles relative to a cloudless sky.

A Cloud optical depth from actinic flux

(Stamnes et al., 1991) described a method to derive the effective cloud optical depth from global spectral irradiance measurements. By effective cloud optical depth is meant the optical depth that when used in the model best reproduces the measurements. Hence, the effective cloud optical depth includes both aerosol and cloud optical depths. The model cloud is assumed to be plane-parallel. The real cloud, however, may consist of broken clouds. In such cases the inferred optical depth is interpreted as the equivalent stratified cloud optical depth consistent with the observations.

During ALBATROSS no UV and/or visible irradiance measurements with a high time frequency were available. Hence, the actinic flux was used to infer the effective cloud optical depth. However, to use the actinic flux is less straightforward than the irradiance.

For increasing effective cloud optical depth the downwelling irradiance at the surface decreases for all solar zenith angle (see Figure 2 of (Stamnes et al., 1991)). However, for the actinic flux this is not the case, see Figure 22. To explain this behaviour it is useful to look at the clear sky actinic flux (F) and irradiance (E).

$$F^{tot}_{clear} = F^{dir}_{clear} + F^{dif}_{clear} = E^{dir}_{clear}/\mu_0 + 2E^{dif}_{clear}. \tag{1}$$

Here μ_0 is the cosine of the solar zenith angle. For simplicity the diffuse radiation field is assumed to be isotropic. Hence the factor 2 in front of E^{dif}_{clear}. For a cloudless sky this factor typically varies between 1.5 and 2.5 depending on solar zenith angle and wavelength.

Clouds reduce the direct irradiance by

$$E^{dir}_{cloudy} = E^{dir}_{clear} \exp(-\tau/\mu_0) \tag{2}$$

where τ is the cloud optical depth. The amount of direct irradiance that is scattered is thus

$$E^{dir}_{clear}(1 - \exp(-\tau/\mu_0)). \tag{3}$$

For thin clouds and single scattering a fraction g is scattered in the foreward direction and a fraction $(1-g)$ in the backward direction. Hence the direct irradiance is reduced by

$$\Delta E^{dir} = -E^{dir}_{clear}(1 - \exp(-\tau/\mu_0)) \tag{4}$$

and the diffuse downward irradiance is enhanced by

$$\Delta E^{dif} = gE^{dir}_{clear}(1 - \exp(-\tau/\mu_0)). \tag{5}$$

The net loss of downward irradiance becomes

$$(g-1)E^{dir}_{clear}(1 - \exp(-\tau/\mu_0)). \tag{6}$$

The corresponding changes in the actinic fluxes are

$$\Delta F^{dir} = \Delta E^{dir} \tag{7}$$
$$\Delta F^{dif} = 2\Delta E^{dif} \tag{8}$$

and the net change in the actinic flux for thin clouds is

$$(2g-1)E^{dir}_{clear}(1 - \exp(-\tau/\mu_0)) \tag{9}$$

which is always positive for $g > 0.5$, while the corresponding relationship for the irradiances, Equation 6, is always negative. Hence the increase in the ratio in Figure 22 for small optical depths and small solar zenith angles.

This implies that the actinic flux may not be used to infer the cloud optical depth for thin clouds and small solar zenith angles.

B Acknowledgements

The author thanks Dr. B. Mayer, DLR, for the explanation of the behaviour of the actinic flux versus effective cloud optical depth.

References

Anderson, G., Clough, S., Kneizys, F., Chetwynd, J., and Shettle, E. (1986). AFGL atmospheric constituent profiles (0-120 km). *Tech. Rep. AFGL-TR-86-0110*, Air Force Geophys. Lab., Hanscom Air Force Base, Bedford, Mass.

Bass, A. M. and Paur, R. J. (1985). The ultraviolet cross–section of ozone, I, The measurements. In Zerefos, C. S. and Ghazi, A., editors, *Atmospheric Ozone: Proceedings of the Quadrennial Ozone Symposium*, pages 606–601. D. Reidel, Norwell, Mass.

Dahlback, A. and Stamnes, K. (1991). A new spherical model for computing the radiation field available for photolysis and heating at twilight. *Planet. Space Sci.*, 39:671–683.

Doda, D. D. and Green, A. E. S. (1980). Surface reflectance measurements in the UV from an airborne platform. Part 1. *Appl. Opt.*, 19:2140–2145.

Hofzumahaus, A., Kraus, A., Kylling, A., and Zerefos, C. (2001). Solar actinic radiation (280-420 nm) in the cloud-free troposphere between ground and 12 km altitude: Measurements and model results. *J. Geophys. Res.*, accepted for publication.

Hofzumahaus, A., Kraus, A., and Müller, M. (1999). Solar actinic flux spectroradiometry: a technique for measuring photolysis frequencies in the atmosphere. *Appl. Opt.*, 38:4443–4460.

Hu, Y. X. and Stamnes, K. (1993). An accurate parameterization of the radiative properties of water clouds suitable for use in climate models. *J. of Climate*, 6:728–742.

Kylling, A., Bais, A. F., Blumthaler, M., Schreder, J., Zerefos, C. S., and Kosmidis, E. (1998). The effect of aerosols on solar UV irradiances during the Photochemical Activity and Solar Ultraviolet Radiation campaign. *J. Geophys. Res.*, 103:26,051–26,060.

Mayer, B., Seckmeyer, G., and Kylling, A. (1997). Systematic long–term comparison of spectral UV measurements and UVSPEC modeling results. *J. Geophys. Res.*, 102:8755–8767.

Nicolet, M. (1984). On the molecular scattering in the terrestrial atmosphere: An empirical formula for its calculation in the homosphere. *Planet. Space Sci.*, 32:1467–1468.

Stamnes, K., Slusser, J., and Bowen, M. (1991). Derivation of total ozone abundance and cloud effects from spectral irradiance measurements. *Appl. Opt.*, 30:4418–4426.

Stamnes, K., Tsay, S.-C., Wiscombe, W., and Jayaweera, K. (1988). Numerically stable algorithm for discrete–ordinate–method radiative transfer in multiple scattering and emitting layered media. *Appl. Opt.*, 27:2502–2509.

Talukdar, R. K., Longfellow, C. A., Gilles, M. K., and Ravishankara, A. R. (1998). Quantum yields of $O(^1D)$ in the photolysis of ozone between 289 and 329 nm as a function of temperature. *Geophys. Res. Lett.*, 25:143–146.

van Weele, M., Martin, T. J., Blumthaler, M., Brogniez, C., den Onter, P. N., Engelsen, O., Lenoble, J., Mayer, B., Pfister, G., Ruggaber, A., Walravens, B., Weihs, P., Gardiner, P. G., Gillotay, D., Haferl, D., Kylling, A., Seckmeyer, G., and Wauben, W. M. F. (2000). From model intercomparison towards benchmark UV spectra for six real atmospheric cases. *J. Geophys. Res.*, 105:4916–4925.

Norwegian Institute for Air Research (NILU)
P.O. Box 100, N-2027 Kjeller, Norway

REPORT SERIES SCIENTIFIC REPORT	REPORT NO. OR 68/2001	ISBN 82-425-1322-8 ISSN 0807-7207	
DATE	SIGN.	NO. OF PAGES 22	PRICE NOK 45.-

TITLE	PROJECT LEADER
Final report for the project "Analysis of airborne- and surface measurements of the actinic flux": Actinic fluxes during ALBATROSS	Arve Kylling NILU PROJECT NO. O-99079
AUTHOR(S) Arve Kylling	CLASSIFICATION * A CONTRACT REF. Dr. Andreas Hofzumahaus

REPORT PREPARED FOR

Forschungszentrum Jülich
D-52425 Jülich
Germany

ABSTRACT

NORWEGIAN TITLE

KEYWORDS

ABSTRACT (in Norwegian)

** Classification*
A Unclassified (can be ordered from NILU)
B Restricted distribution
C Classified (not to be distributed)